Chinese Chemical Letters 36 (2025) 109733

Contents lists available at ScienceDirect

Chinese Chemical Letters

journal homepage: www.elsevier.com/locate/cclet

Formation mechanism of herpetrione self-assembled nanoparticles based on pH-driven method

Yuwen Zhu[a,b,1], Xiang Deng[a,1], Yan Wu[a], Baode Shen[b], Lingyu Hang[a], Yuye Xue[a,*], Hailong Yuan[a,*]

[a] Department of Pharmacy, Air Force Medical Center, PLA, Air Force Medical University, Beijing 100142, China
[b] Key Laboratory of Modern Preparation of Traditional Chinese Medicine, Ministry of Education, Jiangxi University of Chinese Medicine, Nanchang 330004, China

ARTICLE INFO

Article history:
Received 28 December 2023
Revised 21 February 2024
Accepted 25 February 2024
Available online 7 March 2024

Keywords:
Traditional Chinese medicine
Nanoparticles
Herpetrione
Interaction
pH-driven method
Self-assembly
Isothermal titration calorimetry

ABSTRACT

The self-assembled nanoparticles (SAN) formed during the decoction process of traditional Chinese medicine (TCM) exhibit non-uniform particle sizes and a tendency for aggregation. Our group found that the pH-driven method can improve the self-assembly phenomenon of *Herpetospermum caudigerum* Wall., and the SAN exhibited uniform particle size and demonstrated good stability. In this paper, we analyzed the interactions between the main active compound, herpetrione (Her), and its main carrier, *Herpetospermum caudigerum* Wall. polysaccharide (HCWP), along with their self-assembly mechanisms under different pH values. The binding constants of Her and HCWP increase with rising pH, leading to the formation of Her-HCWP SAN with a smaller particle size, higher zeta potential, and improved thermal stability. While the contributions of hydrogen bonding and electrostatic attraction to the formation of Her-HCWP SAN increase with rising pH, the hydrophobic force consistently plays a dominant role. This study enhances our scientific understanding of the self-assembly phenomenon of TCM improved by pH driven method.

Decoction is an efficient form of drug delivery in traditional Chinese medicine (TCM), embodying the holistic perspective of TCM and the concept of syndrome differentiation and treatment. The chemical constituents of TCM originate from diverse sources and possess distinctive structures which are susceptible to molecular recognition during the decoction process, leading to the formation of self-assembled nanoparticles (SAN) through non-covalent bonds, such as electrostatic attraction, van der Waals forces, π-π stacking, and hydrogen bonding [1–8]. The chemical composition of SAN of TCM may involve proteins, polysaccharides, lipids, and small molecule active ingredients [9–11]. Iitsuka *et al.* [12] determined the polysaccharide content in *Astragalus* decoction to be 78% by liquid chromatography-mass spectrometry (LC/MS). Zhao *et al.* [13] reported the polysaccharide content of SAN in Naoluo Xintong decoction as 82.75%, with a protein content of 6.20%. Liang *et al.* [1] isolated SAN from the co-decoction of *Angelica sinensis* and *Astragalus membranaceus*, identifying a total of 43 components, including saponins, flavonoids, amino acids, phthalides, organic acids, and other constituents. The rich chemical composition of SAN of TCM and its nanostructure hold promising potential for efficient drug delivery.

It has been reported in the literature that SAN of TCM promote the absorption of active ingredients in the body and play a crucial role in the efficacy of the decoction [14–16]. Wu *et al.* [17] found that SAN in *Coptis chinensis* decoction had the ability to regulate the tight junctions between intestinal epithelial cells, improving berberine transport through active transport and endocytosis. Wang *et al.* [18] discovered that SAN from the co-decoction of *Coptis chinensis* and liquorice exhibited a stronger inhibition of *S. aureus* proliferation and removal of *S. aureus* biofilm compared to the Decoction and the non-SAN fraction. It can be seen that SAN of TCM is also an important material basis for the efficacy of medicine.

However, the particle size of the SAN obtained from the decoction of TCM is not uniform and is prone to aggregation, which, in turn, affects the efficacy of the drug [10,19]. Our group discovered that the self-assembly process of TCM can be improved through the pH-driven method. In this approach, TCM is initially decocted using a non-neutral solvent. Subsequently, upon adjusting

* Corresponding authors.
E-mail addresses: 1585414032@qq.com (Y. Xue), yhlpharm@126.com (H. Yuan).
[1] These authors contributed equally to this work.

https://doi.org/10.1016/j.cclet.2024.109733
1001-8417/

the decoction to a neutral pH using a pH-adjusting agent, the pH-driven formation of SAN of TCM exhibited uniform particle size and demonstrated good stability.

Our group conducted a preliminary analysis of the formation process of pH-driven SAN in TCM using *Herpetospermum caudigerum* Wall. as a model drug. Given the complex composition of TCM, analyzing the intermolecular forces among its chemical components in detail can be challenging. To address this, we isolated *Herpetospermum caudigerum* Wall. polysaccharide (HCWP), the primary carrier, and herpetrione (Her), the major active components in SAN. Subsequently, we employed the pH-driven method to prepare Her-HCWP SAN (Supporting information methods 2.1) and investigated the interaction between Her and HCWP under varying pH conditions, examining its self-assembly mechanism at different pH levels.

The impact of the Her and HCWP combination at different pH values (9.5–11.5) on the average particle size, zeta potential, and morphology of Her-HCWP SAN was investigated. As depicted in Fig. 1, the average particle size of Her-HCWP SAN decreased with increasing pH. Simultaneously, the negative surface charge of Her-HCWP SAN initially increased and then stabilized. Notably, Her-HCWP $SAN_{11.5}$ exhibited a zeta potential of -53.58 ± 3.69 mV, significantly larger than that of Her-HCWP $SAN_{9.5}$ and Her-HCWP $SAN_{10.0}$ in absolute value. The heightened surface charge of Her-HCWP $SAN_{11.5}$ fosters robust electrostatic repulsion between nanoparticles, reducing aggregation and enhancing stability [20]. Fig. 2 shows the transmission electron microscope (TEM) images of Her-HCWP SAN formed under different pH drives. The Her-HCWP SAN fabricated under high pH values exhibited a spherical-like structure with clear boundaries between particles, while the Her-HCWP SAN fabricated under low pH driving exhibited agglomeration. As shown in Fig. 2E, Her-HCWP $SAN_{11.5}$ demonstrated minimal inter-particle adhesion and no agglomeration. This observation implies that Her-HCWP $SAN_{11.5}$ exhibits superior stability, as supported by the zeta potential results.

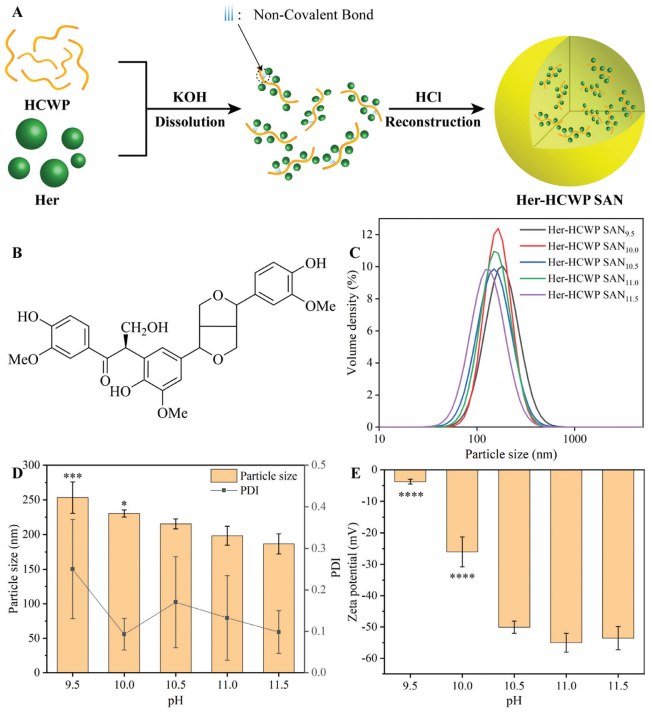

Fig. 1. (A) Schematic illustration of the formation of Her-HCWP SAN by pH-driven method. (B) Chemical structure of Her. (C) The size distribution of Her-HCWP SAN. Effects of different pH drives on (D) particle size, PDI and (E) zeta potential of Her-HCWP SAN. $^{*}P < 0.05$, $^{***}P < 0.001$, $^{****}P < 0.0001$ compared with the pH 11.5 group. Results are shown as mean ± standard deviation (SD) ($n = 3$).

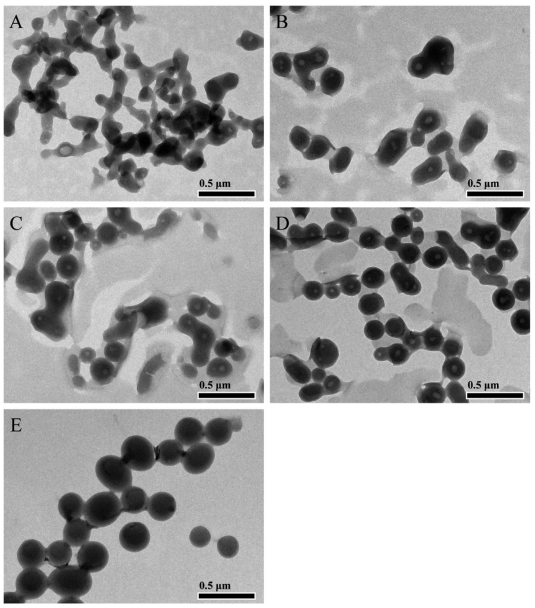

Fig. 2. TEM images of Her-HCWP SAN. (A) Her-HCWP $SAN_{9.5}$, (B) Her-HCWP $SAN_{10.0}$, (C) Her-HCWP $SAN_{10.5}$, (D) Her-HCWP $SAN_{11.0}$, (E) Her-HCWP $SAN_{11.5}$.

The intermolecular interactions between Her and HCWP during the formation of Her-HCWP SAN were investigated using ultraviolet–visible spectroscopy (UV–vis) and Fourier transform infrared spectroscopy (FTIR). As shown in Fig. 3A, the characteristic absorption peaks of Her were at 202, 229, and 280 nm, and those of HCWP were at 199 and 264 nm. After self-assembly, the absorption peak of HCWP at 264 nm disappeared, and the intensities of the absorption peaks of Her at 229 and 280 nm decreased, suggesting that intermolecular interactions between Her and HCWP occurred under alkaline conditions [21]. Fig. 3B illustrates the characteristic peaks of HCWP for amide I (C=O stretching vibration) and amide II (N–H bending vibration and C–N stretching vibration) appeared at 1649 and 1544 cm^{-1}, respectively. When comparing Her-HCWP $SAN_{9.5}$, Her-HCWP $SAN_{10.0}$, Her-HCWP $SAN_{10.5}$, Her-HCWP $SAN_{11.0}$, and Her-HCWP $SAN_{11.5}$ with HCWP, the absorption peaks of amide II shifted from 1544 cm^{-1} to 1551, 1554, 1554, 1555, 1555 cm^{-1} with a reduction in intensity, indicating a potential contribution from the electrostatic interaction between Her and HCWP [22,23]. The absorption peak of Her at 3359 cm^{-1} corresponds to the hydroxyl group's telescopic vibration absorption. However, the absorption peak of the Her-HCWP SAN shifted to 3311 cm^{-1}, indicating the presence of hydrogen bonding interactions during the formation of Her-HCWP SAN [24,25]. Additionally, Her exhibits C–O stretching vibrational absorption peaks at 1271 and 1029 cm^{-1} in aromatic and fatty ethers [26], respectively. Both peaks shift to higher wave numbers after self-assembly. In addition, the intensities of the C–H stretching vibrational absorption peaks in Her-HCWP SAN at 2936 and 2873 cm^{-1} were significantly reduced compared to those in physical mixtures (PM) of Her-HCWP, indicating the presence of hydrophobic interactions during the self-assembly process of Her and HCWP [27]. These findings suggest that hydrogen bonding interactions, hydrophobic forces, and electrostatic attraction are involved in the formation of Her-HCWP SAN.

The thermal stability of Her, HCWP, PM of Her-HCWP and Her-HCWP SAN was assessed through thermogravimetric and thermogravimetric differential curves. As shown in Fig. 4A, the initial weight loss of Her-HCWP SAN (40–115 °C) is attributed to the

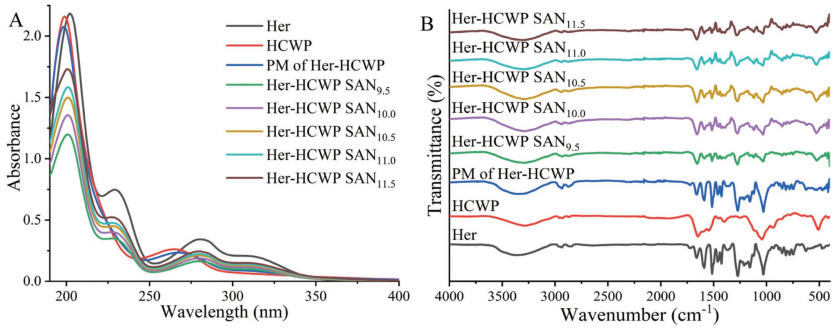

Fig. 3. Spectrograms of Her, HCWP, PM of Her-HCWP, Her-HCWP $SAN_{9.5}$, Her-HCWP $SAN_{10.0}$, Her-HCWP $SAN_{10.5}$, Her-HCWP $SAN_{11.0}$, Her-HCWP $SAN_{11.5}$. (A) The ultraviolet and visible absorption spectroscopy. (B) The Fourier transform infrared spectroscopy.

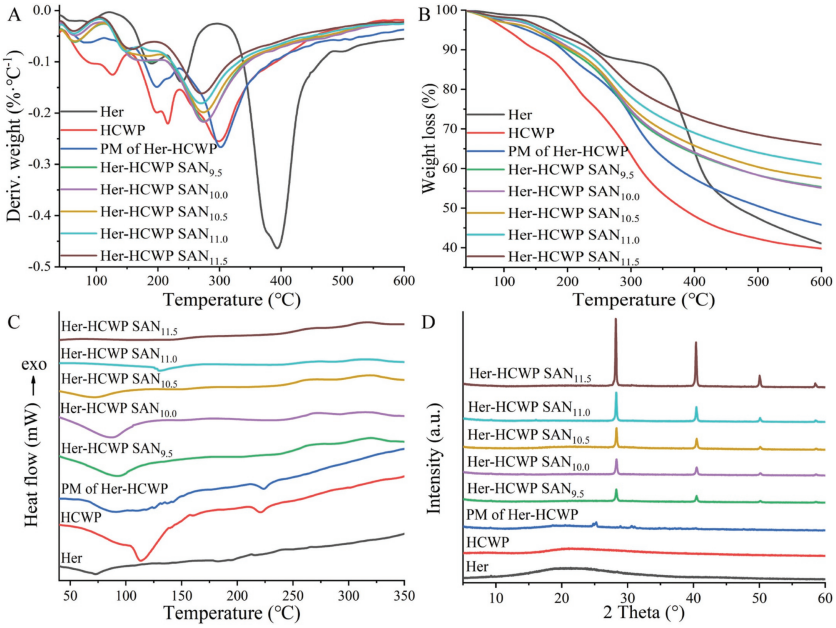

Fig. 4. Physicochemical properties of Her, HCWP, PM of Her-HCWP, Her-HCWP $SAN_{9.5}$, Her-HCWP $SAN_{10.0}$, Her-HCWP $SAN_{10.5}$, Her-HCWP $SAN_{11.0}$, Her-HCWP $SAN_{11.5}$. (A) Thermogravimetry analysis thermograms. (B) Derivative thermogravimetry curves. (C) Differential scanning calorimetry curves. (D) X-ray diffraction spectra.

evaporation of water. The subsequent weight loss (220–350 °C) is more concentrated compared to the broader range observed in the PM of Her-HCWP (160–420 °C), indicating intermolecular assembly and rearrangement. Analysis of the thermogravimetric curves reveals that, at 600 °C, the total weight loss of Her-HCWP SAN is lower than that of Her and HCWP, indicating enhanced thermal stability through self-assembly [28]. Specifically, at 600 °C, Her-HCWP $SAN_{9.5}$ exhibited a 45% weight loss, while Her-HCWP $SAN_{11.5}$ showed only 35%, indicating the higher thermal stability achieved by preparing Her-HCWP SAN at high pH values.

The thermal analysis of Her, HCWP, PM of Her-HCWP, and Her-HCWP SAN is depicted in Fig. 4C. The PM of Her-HCWP exhibited an endothermic band in the temperature range of 70–150 °C, corresponding to the dehydration process. In comparison, the band of adsorption associated with the dehydration process in Her-HCWP SAN shifted to a lower temperature and was less endothermic. Additionally, the degradation heat absorption peak of HCWP at 225 °C disappeared from the differential scanning calorimetry (DSC) curves of Her-HCWP SAN, suggesting changes in water content and thermal stability following the self-assembly of Her with HCWP [29]. Diffraction information of the crystals was obtained using X-ray diffraction (XRD). As shown in Fig. 4D, both Her and HCWP exhibit a broad diffraction peak at $2\theta = 21.0°$, indicating their amorphous nature. After self-assembly, the $2\theta = 21.0°$ diffraction peak in Her-HCWP SAN decreases or disappears, signifying an enhanced amorphous property [30]. This improvement contributes to increased drug solubility and oral bioavailability [31]. Additionally, the diffraction peaks at $2\theta = 28.2°$, 40.3°, 50.0°, and 58.5° in Her-HCWP SAN correspond to characteristic peaks of KCl, with differences in peak intensity resulting from varying amounts of KCl produced during acid-base neutralization at different pH values in the preparation process [32].

From a thermodynamic perspective, the self-assembly process needs to resist the reduction of free energy and negative entropy components, which must be achieved by weak intermolecular interaction forces [33,34]. To elucidate the forces that maintain the nanostructures, we introduced various chemicals into Her-HCWP SAN solutions prepared at different pH values to determine the intra-particle interaction forces. Tris-glycine buffer disrupts electrostatic interactions, sodium dodecyl sulfate (SDS) disrupts hydrophobic interactions, and urea acts as a hydrogen bond disruptor [35]. As illustrated in Fig. 5, the particle sizes of Her-HCWP SAN prepared at different pH values exhibited a significant increase with the addition of SDS, underscoring the substantial impact of hydrophobic interactions on Her-HCWP SAN at different pH values. Notably, Her-HCWP $SAN_{11.5}$ displayed a smaller change in particle size after the addition of SDS compared to other Her-HCWP SAN groups, possibly indicating a weakened hydrophobic interaction

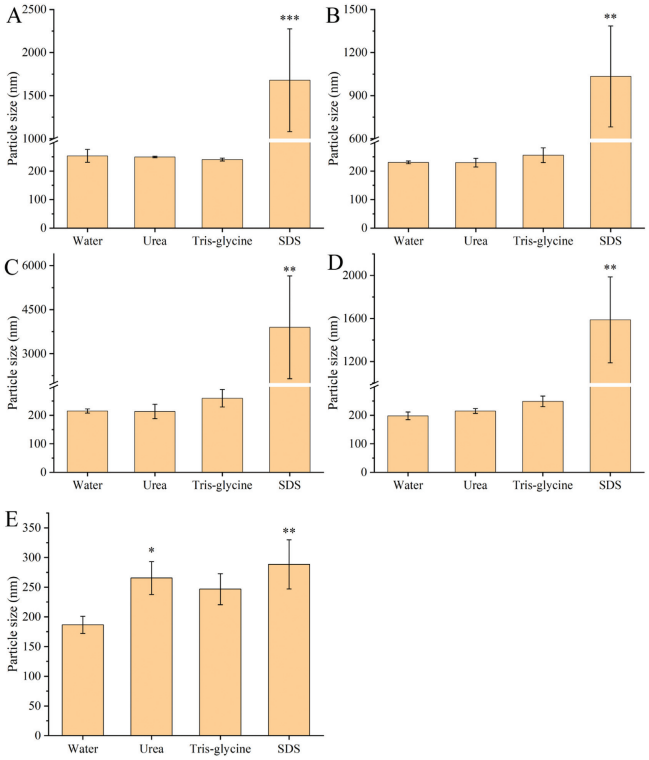

Fig. 5. Effects of the presence of urea, Tris-glycine, and SDS on the particle size of the Her-HCWP SAN prepared under different pH drives. (A) Her-HCWP $SAN_{9.5}$, (B) Her-HCWP $SAN_{10.0}$, (C) Her-HCWP $SAN_{10.5}$, (D) Her-HCWP $SAN_{11.0}$, (E) Her-HCWP $SAN_{11.5}$. $^{*}P < 0.05$, $^{**}P < 0.01$, $^{***}P < 0.001$ compared with the water group. Results are shown as mean ± SD ($n = 3$).

force between Her and HCWP at pH 11.5. Furthermore, the particle size of Her-HCWP $SAN_{11.5}$ increased significantly after the addition of urea, highlighting the substantial role of hydrogen bonding in the formation of Her-HCWP $SAN_{11.5}$ at this stage. In contrast, Her-HCWP $SAN_{9.5}$, Her-HCWP $SAN_{10.0}$, Her-HCWP $SAN_{10.5}$, and Her-HCWP $SAN_{11.0}$ showed no significant changes in particle size after the addition of Tris-glycine buffer and urea. This indicates that hydrogen bonding and electrostatic attraction do not play a dominant role in the binding of Her to HCWP within the pH range of 9.5–11.0.

To further explore the binding behavior of Her and HCWP at different pH values, the thermodynamic parameters of the interaction between Her and HCWP at 25 °C were determined using the isothermal titration calorimetry (ITC) method. As can be seen from Fig. 6, the heat flow is negative at all pH values, indicating that the interaction between Her and HCWP is exothermic and becomes more exothermic with increasing pH values. Computer simulations of the microthermal titration data were carried out by Nano ITC analysis software and the obtained thermodynamic parameters are summarized in Table 1. As observed in Table 1, ΔG was less than 0 at different pH values, indicating that the binding of Her to HCWP was spontaneous. ΔG was much lower than the energy of covalent bond formation (about −95.56 kcal/mol), suggesting that the binding of Her to HCWP occurs via non-covalent bonds [35,36]. While ΔG decreases with increasing pH values, the change is not significant. This phenomenon may be attributed to the occurrence of an enthalpy-entropy compensation effect, where a decrease in one factor is compensated by an increase in the other factor [37–39]. $\Delta H < 0$ and $\Delta S > 0$ for Her binding to HCWP suggests that the binding of the two molecules is driven by enthalpy and entropy. The ΔH of the system decreased with increasing pH values, and the ΔH at pH 11.5 was 2.87 times higher than the ΔH at pH 9.5, suggesting that the importance of electrostatic attraction, hydrogen bonding, and van der Waals' forces in the binding of the two molecules increased with increasing pH [40]. However, the absolute value of $-T\Delta S$ is much larger than that of ΔH at all pH values, indicating that ΔS, determined by hydrophobic interactions, plays a dominant role in the binding of the two molecules [41,42]. Additionally, temperature and salt ion strength play crucial roles in the self-assembly process of Her with HCWP. The rise in temperature, coupled with an increase in salt ionic strength, results in a decrease in the K_a value of Her and HCWP,

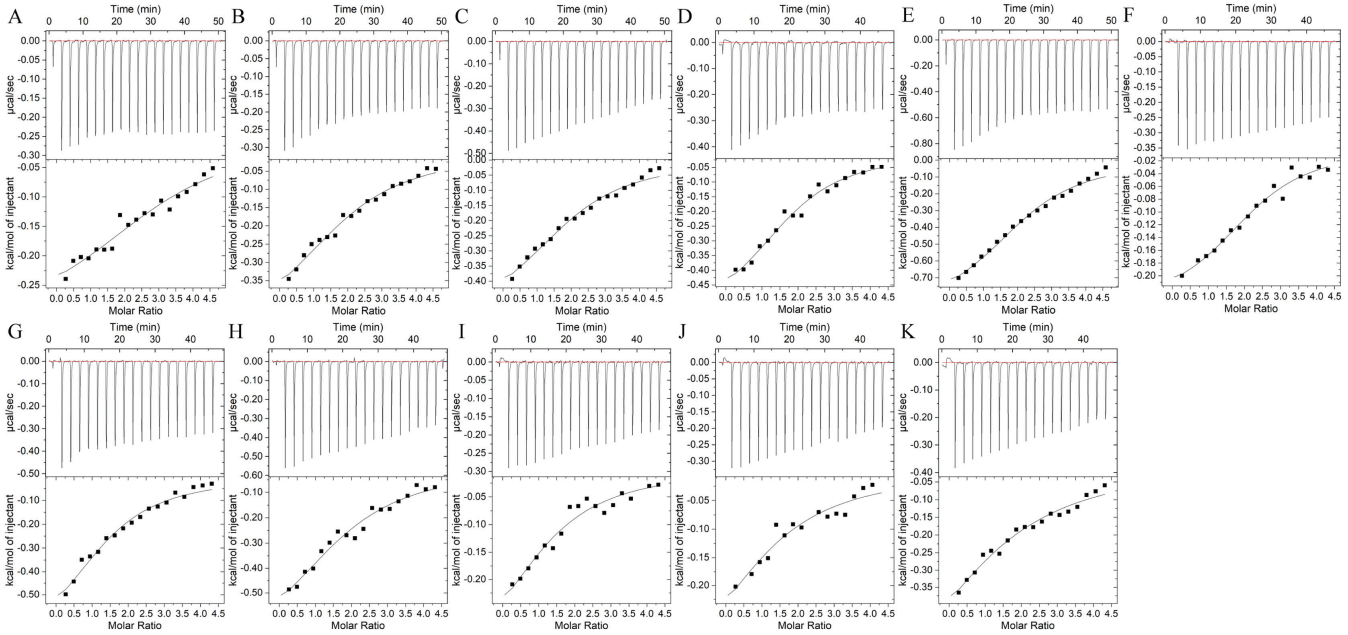

Fig. 6. Thermograms (top panels) and binding isotherms (bottom panels) corresponding to the titration of the Her (4.53 μmol/L) with HCWP (0.0625 μmol/L) in CAPS buffer (20 mmol/L) at various pH levels, temperatures, and salt ionic strengths. 25 °C, 0 mmol/L NaCl, pH 9.5 (A), pH 10.0 (B), pH 10.5 (C), pH 11.0 (D), and pH 11.5 (E); pH 11.0, 0 mmol/L NaCl, 15 °C (F), 35 °C (G), and 45 °C (H); pH 11.0, 25 °C, 20 mmol/L NaCl (I), 50 mmol/L NaCl (J), and 100 mmol/L NaCl (K).

Table 1
Thermodynamic parameters (affinity constant (K_a), enthalpic contribution (ΔH), entropic contribution ($T\Delta S$) and Gibbs free energy (ΔG)) of binding between Her and HCWP upon pH, temperature, and salt ion strength.

pH	Temp (°C)	NaCl (mmol/L)	$K_a \times 10^4$ (L/mol)	ΔH (cal/mol)	$T\Delta S$ (cal/mol)	ΔG (cal/mol)
9.5	25	0	0.70 ± 0.30	-314.1 ± 47.7	4946.8	−5260.9
10.0	25	0	0.83 ± 0.18	-507.7 ± 57.8	4827.6	−5335.3
10.5	25	0	1.02 ± 0.22	-538.1 ± 53.6	4917.0	−5455.1
11.0	25	0	1.27 ± 0.30	-575.6 ± 58.6	5006.4	−5582
11.5	25	0	1.32 ± 0.21	-901.5 ± 52.4	4708.4	−5609.9
11.0	15	0	1.59 ± 0.40	-247.9 ± 20.97	5299.2	−5547.1
11.0	35	0	0.98 ± 0.25	-794.0 ± 129.3	4835.6	−5629.6
11.0	45	0	0.75 ± 0.25	-804.3 ± 156.8	4833.6	−5637.9
11.0	25	20	0.69 ± 0.32	-427.3 ± 166.0	4797.8	−5225.1
11.0	25	50	0.51 ± 0.31	-463.7 ± 286.3	4589.2	−5052.9
11.0	25	100	0.35 ± 0.14	-893.2 ± 391.9	3933.6	−4826.8

thereby significantly influencing the morphology of Her-HCWP SAN [43].

In summary, we systematically investigated the interactions of Her and HCWP and their self-assembly mechanisms at different pH values through thermodynamic and multispectral analysis. With increasing pH, the interaction force between Her and HCWP strengthens, resulting in a stronger binding and the formation of Her-HCWP SAN characterized by a smaller particle size, higher zeta potential, more regular morphology, and improved thermal stability. Her-HCWP SAN formation involved hydrogen bonding, electrostatic attraction, and hydrophobic forces. The strengthening of hydrogen bonding and electrostatic attraction with increasing pH values is noteworthy. Importantly, the role of ΔS, influenced by hydrophobic interactions, is crucial in governing the binding between the two molecules. At higher pH levels, the binding constants of Her and HCWP increase, and the process becomes more exothermic, significantly contributing to the stability of Her-HCWP SAN. This study deepens our understanding of the interactions between small-molecule active ingredients and macromolecules in TCM across various pH values. Moreover, it elucidates the scientific principles of pH-driven enhancements in TCM self-assembly phenomena. This study provides valuable insights for controlling and improving the self-assembly phenomenon of TCM, facilitating its application in the pharmaceutical industry.

Declaration of competing interest

The authors declare that they have no known competing financial interests or personal relationships that could have appeared to influence the work reported in this paper.

Acknowledgment

This work was supported by the National Natural Science Foundation of China (Nos. 81873092, 82174074).

Supplementary materials

Supplementary material associated with this article can be found, in the online version, at doi:10.1016/j.cclet.2024.109733.

References

[1] P. Liang, T. Bi, Y. Zhou, et al., ACS Appl. Mater. Interfaces 15 (2023) 47939–47954.
[2] Y. Hou, L. Zou, Q. Li, et al., Mater. Today Bio 15 (2022) 100327.
[3] Y. Xu, J. Chen, S. Shi, et al., Carbohydr. Polym. 303 (2023) 120452.
[4] Q. Pei, B. Jiang, D. Hao, Z. Xie, Acta Pharm. Sin. B 13 (2023) 3252–3276.
[5] L. Hang, C. Shen, B. Shen, H. Yuan, Chin. Chem. Lett. 33 (2022) 4948–4951.
[6] C.L. Yao, J.Q. Zhang, J.Y. Li, et al., Nat. Prod. Rep. 38 (2021) 1618–1633.
[7] M. Liao, Q. Xie, Y. Zhao, et al., Pharmacol. Res. 176 (2022) 106077.
[8] Y. Jin, H. Pang, L. Zhao, et al., Phytomedicine 107 (2022) 154425.
[9] C.Y. Shen, F. Hu, J.J. Zhu, et al., Chin. J. Chin. Mater. Med. 46 (2021) 4875–4880.
[10] X. Huang, X. Liu, X. Lin, et al., J. Nanobiotechnology 20 (2022) 527.
[11] Z. Li, X. Xu, Y. Wang, L. Kong, C. Han, J. Adv. Res. 50 (2023) 159–176.
[12] H. Iitsuka, K. Koizumi, A. Inujima, et al., Biochem. Biophys. Rep. 16 (2018) 62–68.
[13] G. Zhao, L. Hong, M. Liu, et al., Molecules 27 (2022) 1511.
[14] Y. Gao, Y. Dong, Q. Guo, et al., Molecules 27 (2022) 3268.
[15] H. He, Y. Lu, J. Qi, et al., Acta Pharm. Sin. B 9 (2019) 36–48.
[16] Z. Zhang, Y. Lu, J. Qi, W. Wu, Acta Pharm. Sin. B 11 (2021) 2449–2468.
[17] J. Wu, Y. Yang, X. Yuan, et al., Food Funct. 11 (2020) 10480–10492.
[18] Z. Wang, W. Li, J. Lu, et al., J. Ethnopharmacol. 300 (2023) 115704.
[19] L. Qiao, H. Yang, S. Gao, et al., J. Mater. Chem. B 10 (2022) 1908–1922.
[20] Y. Yuan, M. Ma, S. Zhang, D. Wang, Y. Xu, Int. J. Biol. Macromol. 195 (2022) 302–308.
[21] B. Liu, Y. Vonhausen, A. Schulz, C. Höbartner, F. Würthner, Angew. Chem. Int. Ed. 61 (2022) e202200120.
[22] K. Ma, L. Zhang, X. Sun, F. Chen, T. Zhu, Ultrason. Sonochem. 100 (2023) 106596.
[23] X. Zhao, D. Li, Y.H. Lu, et al., Proc. Natl. Acad. Sci. U. S. A. 119 (2022) e2200019119.
[24] C. Shen, M. Wu, C. Sun, et al., Carbohydr. Polym. 286 (2022) 119267.
[25] L. Tu, M. Cheng, Y. Sun, et al., Int. J. Pharm. 573 (2020) 118730.
[26] Y. Zhu, X. Deng, L. Chen, et al., Acta Pharm. Sin. 59 (2024) 448–454.
[27] M. Javed, H. Huang, Y. Ma, et al., Food Chem. 438 (2023) 137948.
[28] L. Issman, P.A. Kloza, J.Terrones Portas, et al., ACS Nano 16 (2022) 9583–9597.
[29] P.W. Xu, X.J. Yue, X.F. Yuan, B. Zhao, Int. J. Biol. Macromol. 256 (2024) 128380.
[30] B.B. Yan, Y. Zhao, M. Li, et al., Nano Lett. 22 (2022) 9181–9189.
[31] P. Zhao, W. Han, Y. Shu, et al., J. Control. Release 353 (2023) 42–50.
[32] L.X. Wang, L.P. Dao, Q.Y. Guo, et al., Food Chem. 386 (2022) 132755.
[33] X. Zhang, X. Dai, L. Gao, et al., Chem. Soc. Rev. 52 (2023) 6806–6837.
[34] L. Zou, M. Cheng, K. Hu, J. Feng, L. Tu, Chin. Chem. Lett. 35 (2024) 109129.
[35] Y.W. Liu, Q.H. Li, G.Q. Huang, J.X. Xiao, Food Hydrocoll. 137 (2023) 108382.
[36] S. Hafeez, M.C. Decarli, A. Aldana, et al., Adv. Mater. 35 (2023) e2301242.
[37] H. Mizuno, G. Fukuhara, Acc. Chem. Res. 55 (2022) 1748–1762.
[38] T. Walker, H.M. Sun, T. Gunnels, et al., ACS Cent. Sci. 9 (2023) 466–475.
[39] S.M. Wang, Y.F. Wang, L. Huang, et al., Nat. Commun. 14 (2023) 5645.
[40] X. Nai, Y. Chen, S. Hao, et al., J. Chem. Thermodyn. 168 (2022) 106724.
[41] S. Liu, N. Sun, K. Ren, et al., Food Hydrocoll. 148 (2024) 109491.
[42] Y. Lu, Z. Yu, X. Yang, et al., Chin. Chem. Lett. 34 (2023) 108040.
[43] I.D. Lima Cavalcanti, F.H. Xavier Junior, N.S. Santos Magalhães, M.C.D.B. Lira Nogueira, Int. J. Pharm. 641 (2023) 123063.